Supporting Information

Effect of fluoroethylene carbonate on transport property of the electrolyte towards Ni-rich Li-ion batteries with high safety

Salatan Duangdangchote, Nutthaphon Phattharasupakun, Praeploy Chomkhuntod, Poramane Chiochan, Sangchai Sarawutanukul, Chanikarn Tomon, and Montree Sawangphruk[*]

Center of Excellence for Energy Storage Technology (CEST), Department of Chemical and Biomolecular Engineering, School of Energy Science and Engineering, Vidyasirimedhi Institute of Science and Technology, Rayong 21210, Thailand
Corresponding author. E-mail address: montree.s@vistec.ac.th (M. Sawangphruk).

Classical molecular dynamic (MD) simulation details

The classical molecular dynamics (MD) simulations were developed by the optimized potentials for liquid simulations for all-atom (OPLS-AA)[1-4] force field methods for the bond relations (bonds, angles, dihedrals, and impropers). The partial atomic charges for all molecules were obtained by firstly optimizing the geometry using Becke's three parameter exchange function combined with the Lee–Yang–Parr correlation functional (B3LYP)[5] based on the density functional theory (DFT) with the aug-cc-pvdz basis set using the Gaussian 16 simulation package.[6] After that, the electrostatic potential surface was fitted by the RESP[7, 8] method. The simulation cubic boxes were constructed with randomly placed 52 Li^+, 52 PF_6^-, and 600 total carbonate solvent molecules (EC, EMC, DEC, and/or FEC) using PACKMOL[9]. The final concentration of the solution systems is 1.0M lithium salt. The system was equilibrated in a cubic box with periodicity in *x*, *y*, and *z* directions. The initial configuration was energy minimized with a conjugate gradient algorithm for 20,000 steps. By following the minimization, the system was equilibrated with the isothermal-isobaric ensemble at constant number of particles N, pressure P, and temperature T (NPT) for 2 ns with a time step of 0.5 fs and the temperature of 298 K. For production runs, 20 ns simulations at 300 K were carried out in the

constant number of particles N, volume V, and temperature T (NVT) with the Nosé-Hoover chain (NHC)[10] thermostat with a time step of 1 fs and the temperature of 298 K. The last 4 ns of the production runs were used for the MD analysis in this publication. All classical MD simulations were performed with the GROMACS[11-16] simulation package on a 24-cores Unix-based cluster.

Stokes−Einstein relation and mean square displacement (MSD) analysis

In molecular dynamic simulations, the self-diffusion coefficient (*D*) and transference number can be computed from the mean square displacement (MSD) analysis through the Stokes−Einstein relation:

$$D = \frac{1}{6} \times \lim_{t \to \infty} \left(\frac{\langle |\vec{r}(t) - \vec{r}(0)|^2 \rangle}{t} \right)$$

where D is the self-diffusion coefficient of specific ions, $\vec{r}(t)$ is the location of the center of mass of a specific ion at time t. The brackets indicate the ensemble average.

In addition, D of Li^+ and PF_6^- ions can be used to compute the Li^+ and PF_6^- transference number from these following equations:

$$t_{Li^+} = \frac{D_{Li^+}}{D_{Li^+} + D_{PF_6^-}}$$

$$t_{PF_6^-} = 1 - t_{Li^+}$$

where t_{Li^+} and $t_{PF_6^-}$ is the Li^+ and PF_6^- transference number, respectively.

Radial pair distribution function (RPDF) analysis

The structure analysis from the MD simulations can be described with the radial pair distribution function *g(r)*, which quantifies correlation between atom pairs *i* and *j*:

$$g_{ij}(r) = \frac{1}{4\pi r^2}\frac{1}{N\rho}\sum_{i=1}^{N}\sum_{j\neq i}^{N}\left\langle \delta(|r_{ij}| - r)\right\rangle$$

The coordination number *n(R)* over the specific distance *R* of specific ions can be obtained via this following integral:

$$n(R) = 4\pi\rho_j \int_0^R r^2 g_{ij}(r)dr$$

where *r* is the location of the center of mass of a specific ion.

First-principles DFT calculation details

The density functional theory (DFT) investigations in this article were performed by the Gaussian16 computational package[6]. Full optimizations, geometries and property calculations for the total energies were accounted by Becke's three parameter exchange function combined with the Lee–Yang–Parr correlation functional (B3LYP)[5] and the polarized triple ζ basis set 6-311++G(2d,2p) was set for all atoms. The convergence thresholds for self-consistency-field (SCF) were set at 10^{-6} Hartree. All stationary points were characterized as no imaginary frequencies by the calculation using the same level of theory.

Natural bond orbital (NBO) methods

The natural bond orbital (NBO)[17] method was also used to analyze the atomic charge distribution and charge transfer between solvation complex of Li^+, PF_6^- and relevant solvent species. The effect of the environment on the solvation shell was estimated using the polarized continuum models (PCM) with the acetone parameters.[18-20]

Boltzmann distribution and contact ion pair (CIP) formation free energy

The CIP formation energy can be estimated by applying the Boltzmann factor by following equation:

$$\Delta_f G_{CIP} = -k_B T \ln\left(\frac{p(CIP)}{p(SSIP)}\right)$$

where p is the population of specific species, k_B is the Boltzmann constant, and T is the temperature.

Cylindrical 18650-type preparation, fabrication, and electrochemical measurements

All the manufacturing processes were handled within the ISO Class 7 (FED class 10000) clean room with dehumidification systems (controlled within −40 to −55 °C dew point at 25 °C, or relative humidity between 0.60 to 0.11%). The raw materials were characterized by D8 Advance XRD machine for XRD, and Bruker S4 Pioneer for XRF analysis. The cathode slurry was prepared by mixing of active materials NCA ($LiNi_{0.88}Co_{0.09}Al_{0.03}O_2$), Super P conductive, and PVDF binder in a weight ratio of 95.2:2.4:2.4 and homogenized in N-methyl-2-pyrrolidone (NMP) within the 10L vacuum mixer for 12 h. The anode slurry was mixed from graphite, Super P conductive, CMC, and SBR binder in a weight ratio of 95.4:0.9:1.2:2.5 and homogenized in water and ethanol. The slurries were uniformly coated on aluminium (Al) foil substrates for cathode and copper (Cu) foil for anode via separated automatic roll to roll coating machine and immediately dried at 140 °C in which cathode thickness of *ca.* 220 μm and anode thickness of *ca.* 200 μm. After that, the as-coated electrodes were then processed through rolling press, slitting, cutting, winding with trilayer PP/PE/PP separator, electrolyte injection, and crimping. The schematic workflow has been shown in **Figure S0**. The final active NCA weight is in a

range of 14.0 to 15.0 g. The final active graphite weight is in a range of 8.10 to 8.30 g. Precisely 5.0 g of the electrolyte (1M $LiPF_6$ dissolved in EC/EMC/DEC and/or FEC) was injected using the automatic electrolyte injection chamber. After fabrication process, the cell was operated via galvanostatic charge/discharge measurements on BTS-4000 (Neware Technology, Shenzhen, China). The formation process was carried out via multi-step-constant-current (MSCC) from open circuit potential to 4.0V with a constant current of C/25, C/16, C/12.5, and C/10, respectively. For the rate capability investigation, the cells were tested with constant-current-constant-voltage (CCCV) charge to 4.3V and discharge to 3.0V at a current density of C/10, C/4, C/2, C/1, C/0.5, C/0.25, and back to C/10, respectively. For the long-term cycling stability, the cells were cycled with constant-current-constant-voltage (CCCV) charge to 4.2V and discharge to 3.0V at a rate of C/1. The overpotential was calculated for capacity *i* from the following equation:

$$Overpotential(i) = \frac{\left(V_{charge,i} - V_{discharge,i}\right)}{2}$$

Then the data was plotted between the overpotential versus the charge voltage.

UN38.3-T6: Testing needed for lithium-ion battery and/or cells prior to transportation according to UN Manual Transport of Dangerous Goods (Impact test)

The safety test in this article was following the procedures for the impact test for lithium-ion battery cells. The test simulated the mechanical abuse from an impact that may result in an internal short circuit. The test sample cell had been placed on a flat smooth surface in an explosion proof chamber (**Figure S14**, Gelon Lib., China). A 15.8 mm diameter and 61 cm long Type 316 stainless steel bar was set across the center of the sample. The test has started when the 9.1 kg mass to be dropped from a height of 61 cm at the intersection of the bar and sample while the falling mass has been guided to be oriented 90 degrees from the horizontal supporting surface. The cells were observed for possible disassembly, rupture, and/or fire within six hours from the impact. The cells were sampled from the as-fabricated cells after the formation process. The cells were fully charged to 100% SoC via CCCV to 4.3V. Due to the unavailable of the temperature sensor inside the chamber, the isolated mirror glass also blocking an infrared

camera, and for safety concerns we do not open the chamber prior to six hours thus the final temperature does not be able to measure.

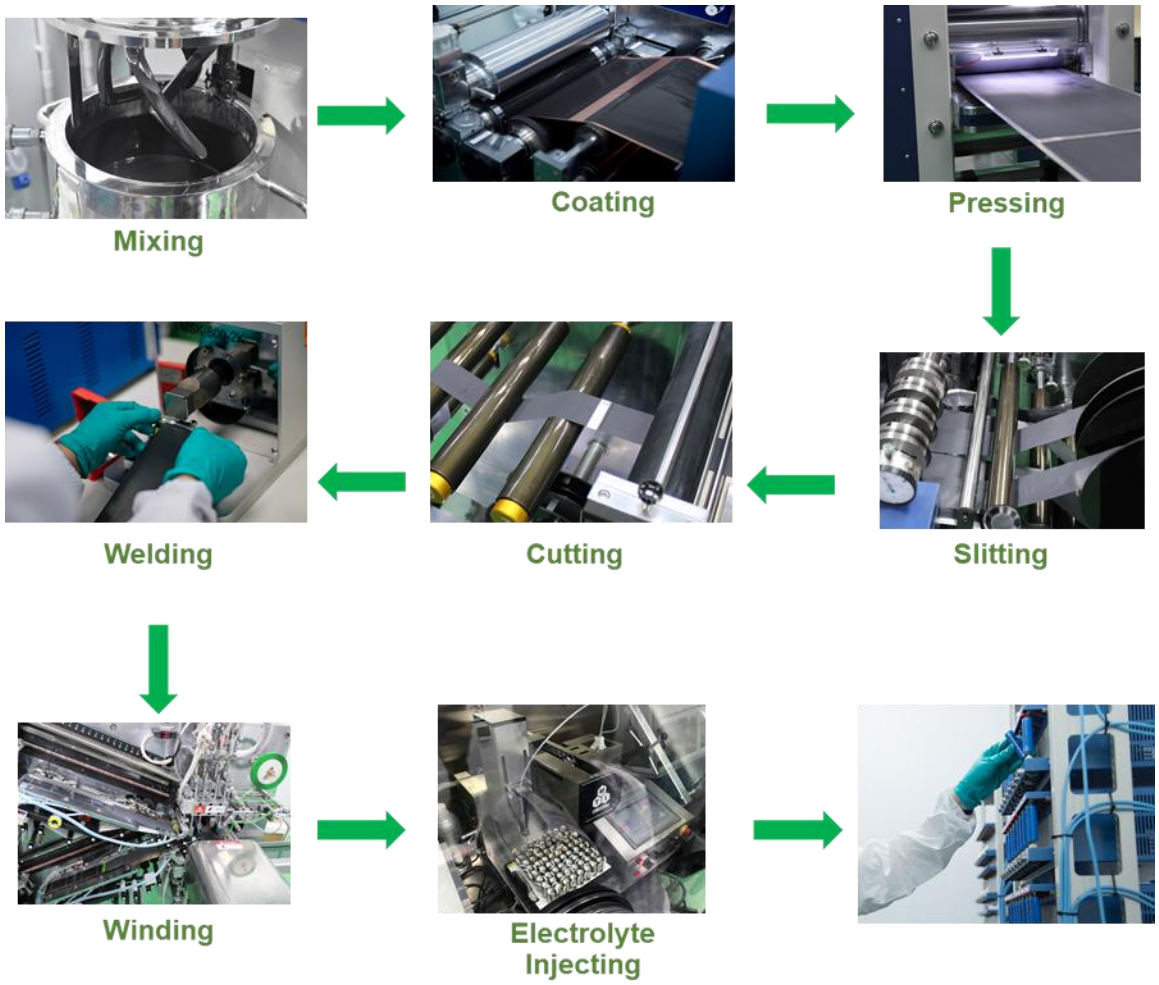

Figure S0. Schematic workflow for fabricating 18650 cell LiBs in this publication.

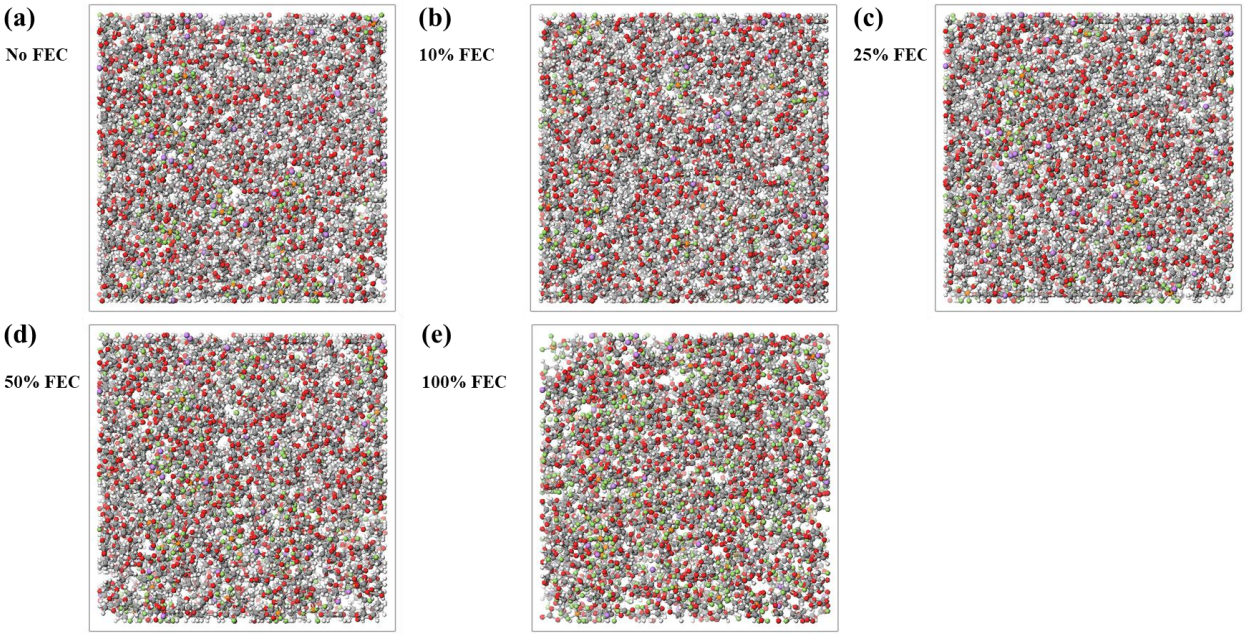

Figure S1. Initial configuration snapshot of the simulation cell for (a) no FEC, (b) 10% FEC, (c) 25% FEC, (d) 50% FEC, and (e) 100% FEC.

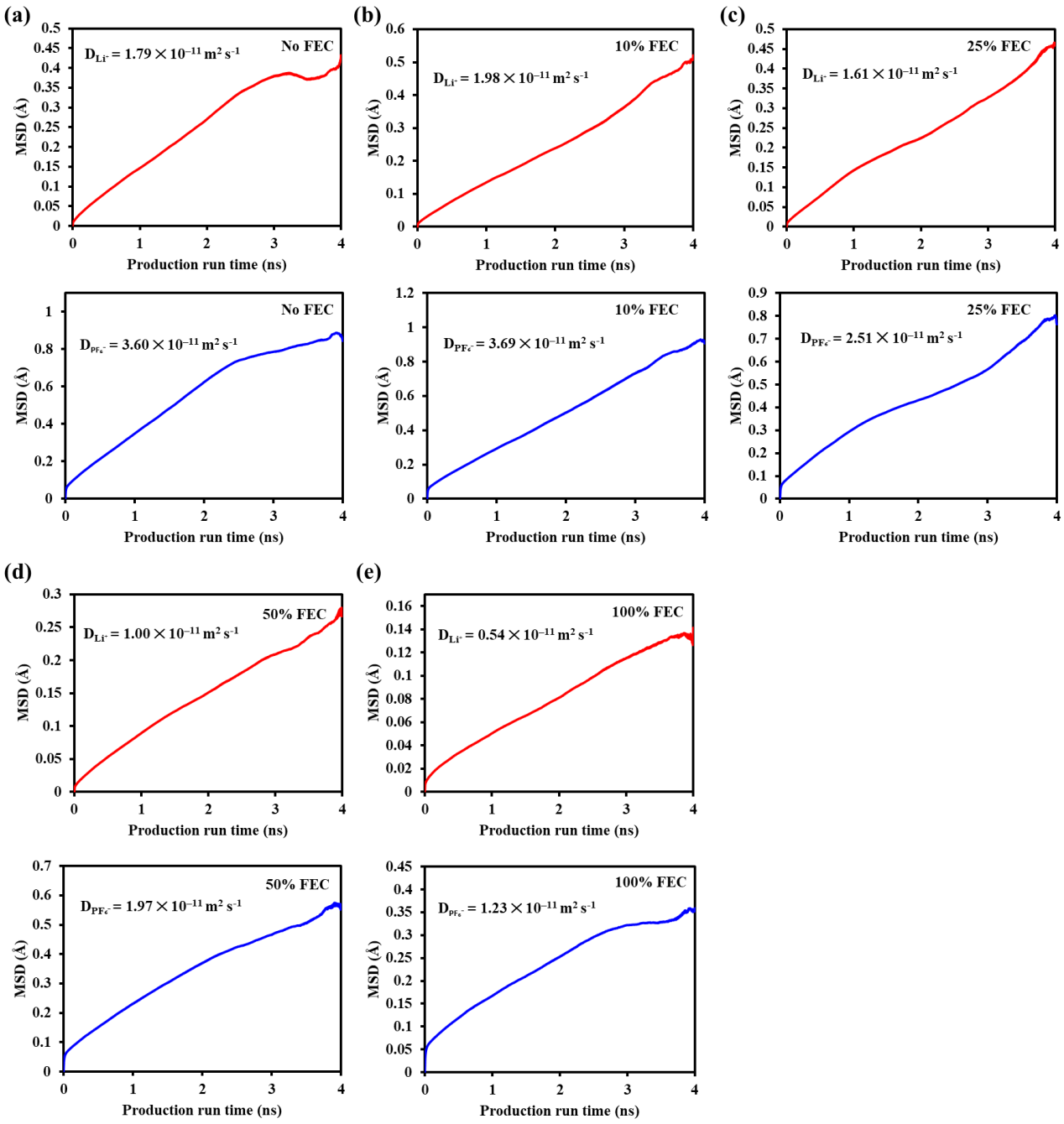

Figure S2. Mean square displacement (MSD) of MD trajectories based on the Stoke-Einstein relation for (a) no FEC, (b) 10% FEC, (c) 25% FEC, (d) 50% FEC, and (e) 100% FEC.

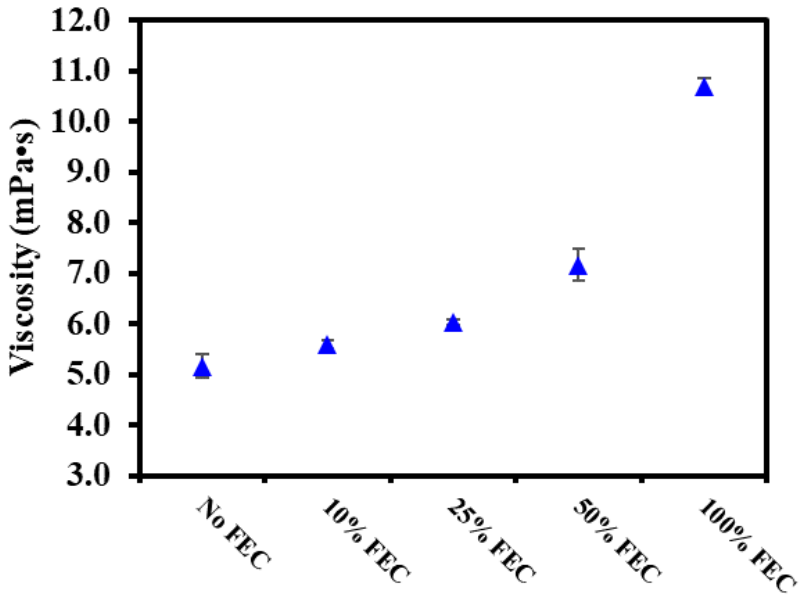

Figure S3. Viscosity measured by a digital viscosity tester. The error bars represent a standard deviation of the data collected three times.

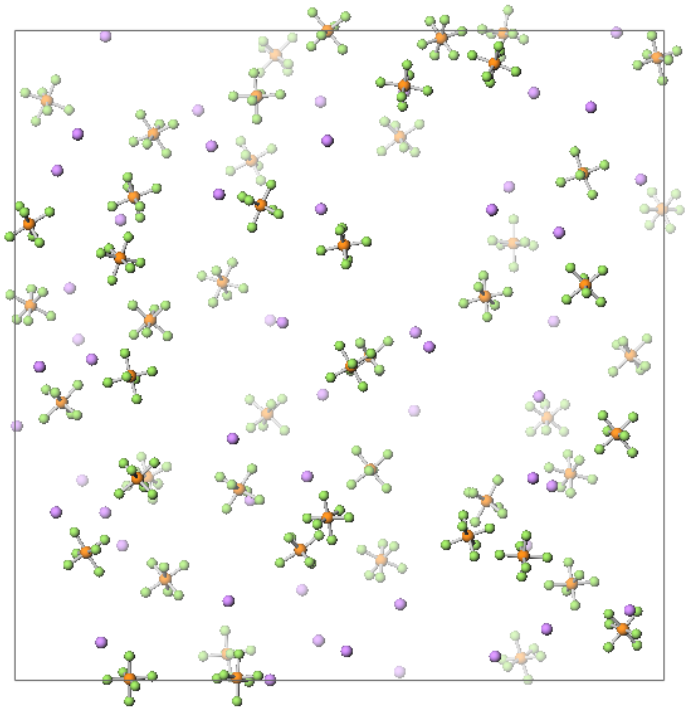

Figure S4. Snapshot of the simulation box from MD simulations without solvent molecules, captured from 25% FEC simulation systems at 20 ns. Purple, green, and orange denote lithium, fluorine, and phosphorus atoms, respectively.

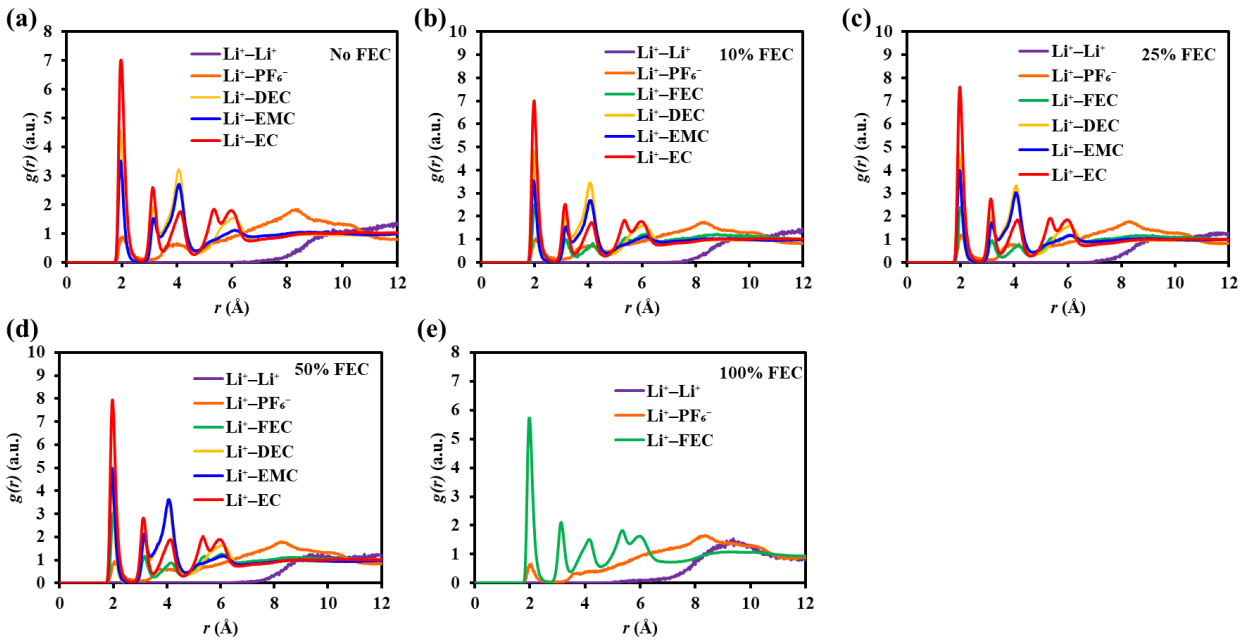

Figure S5. Radial pair distribution function *g(r)* of Li^+ with Li^+, PF_6^-, EC, DEC, EMC, and FEC for (a) no FEC, (b) 10% FEC, (c) 25% FEC, (d) 50% FEC, and (e) 100% FEC.

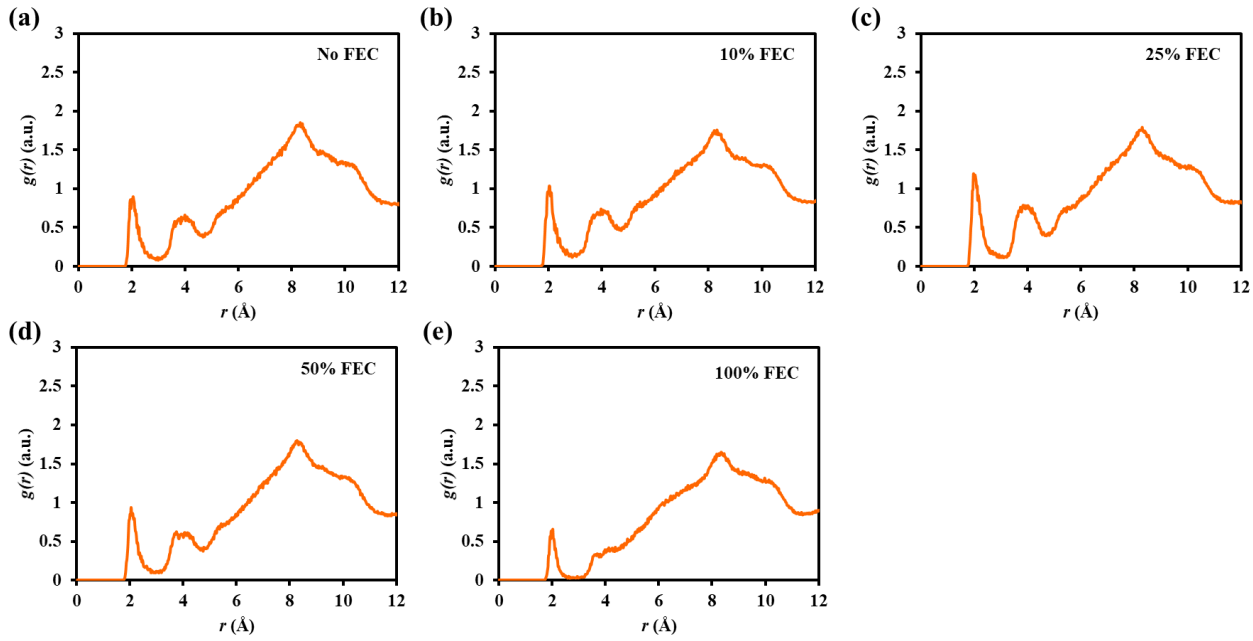

Figure S6. Radial pair distribution function *g(r)* of Li^+ with PF_6^-, for (a) no FEC, (b) 10% FEC, (c) 25% FEC, (d) 50% FEC, and (e) 100% FEC.

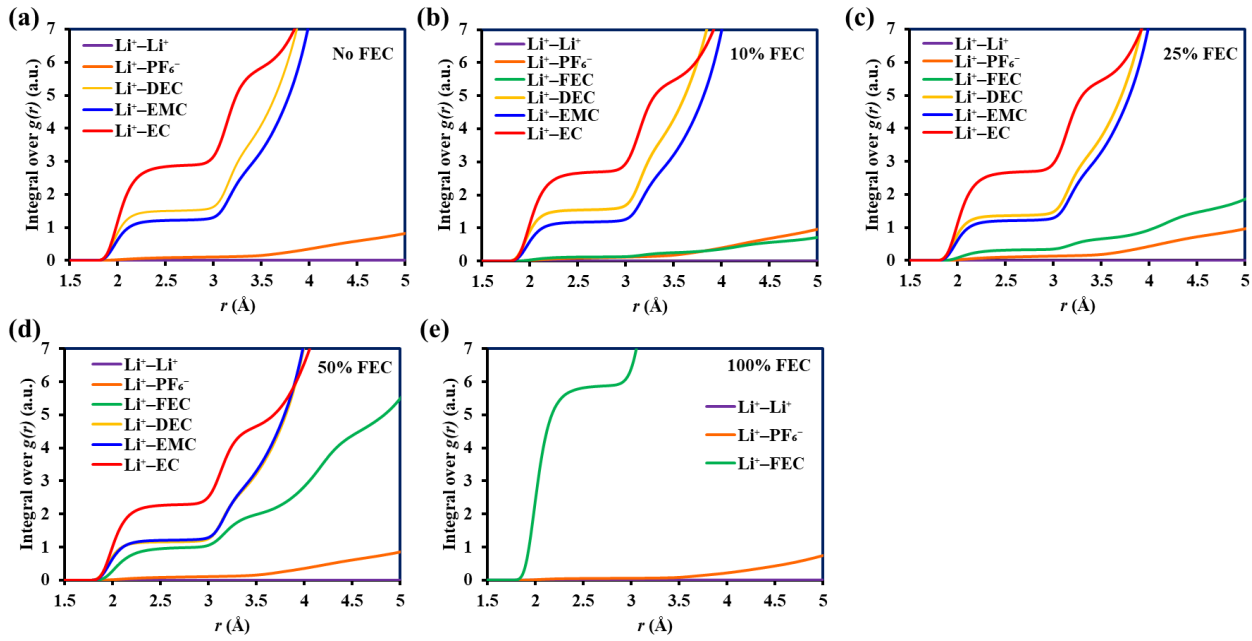

Figure S7. Integral over *g(r)* of Li^+ with Li^+, PF_6^-, EC, DEC, EMC, and FEC for (a) no FEC, (b) 10% FEC, (c) 25% FEC, (d) 50% FEC, and (e) 100% FEC.

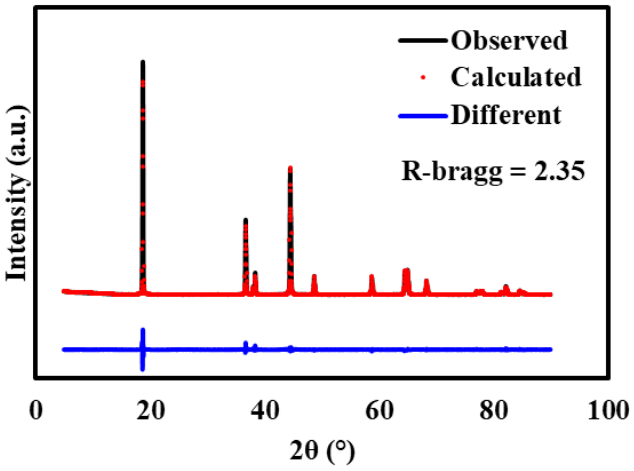

a (Å)	2.868
c (Å)	14.488
z_{oxy}	0.258
Li^{+} at 3a site	0.998
Ni^{2+} at 3a site	0.002

Figure S8. X-ray diffraction (XRD) pattern of a Ni-rich $LiNi_{0.88}Co_{0.09}Al_{0.03}O_2$ raw material and the corresponding Rietveld refinement of the sample.

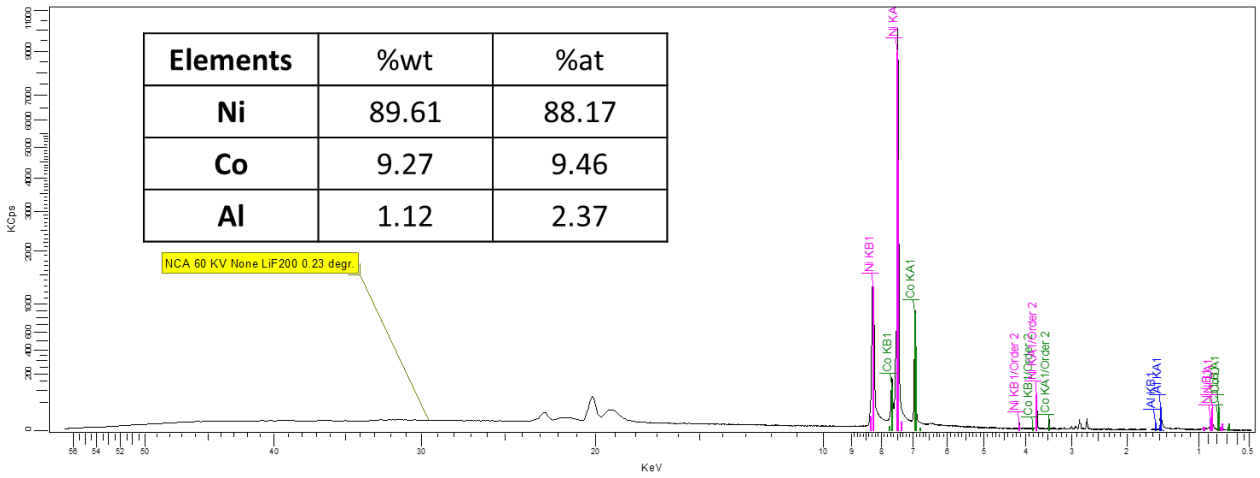

Figure S9. X-ray fluorescence spectrum of Ni-rich $LiNi_{0.88}Co_{0.09}Al_{0.03}O_2$ raw material.

Figure S10. As-fabricated cylindrical 18650-type lithium-ion battery.

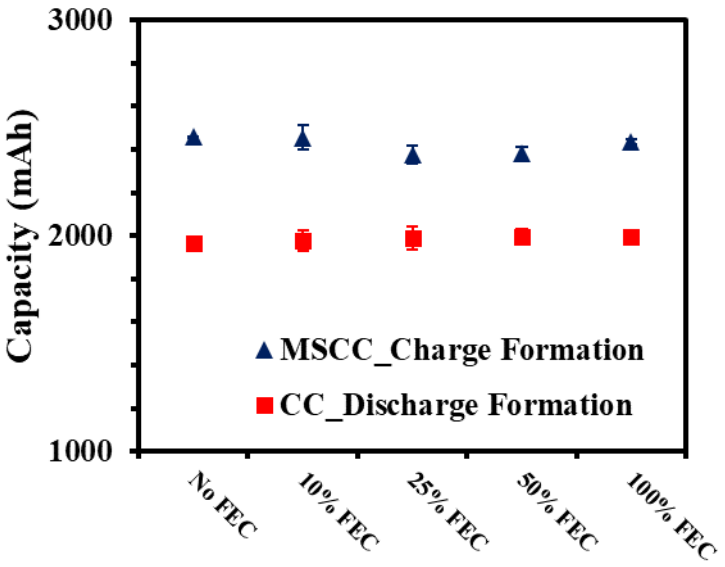

Figure S11. An averaged formation charge/discharge capacity. The error bars represent a standard deviation of the data collected for five cells.

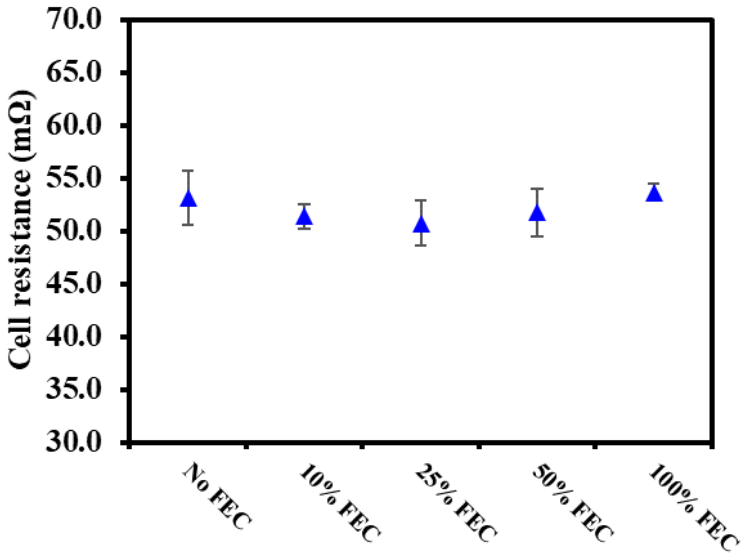

Figure S12. An averaged internal cell resistance measured by battery internal resistance tester. The error bars represent a standard deviation of the data collected for five cells.

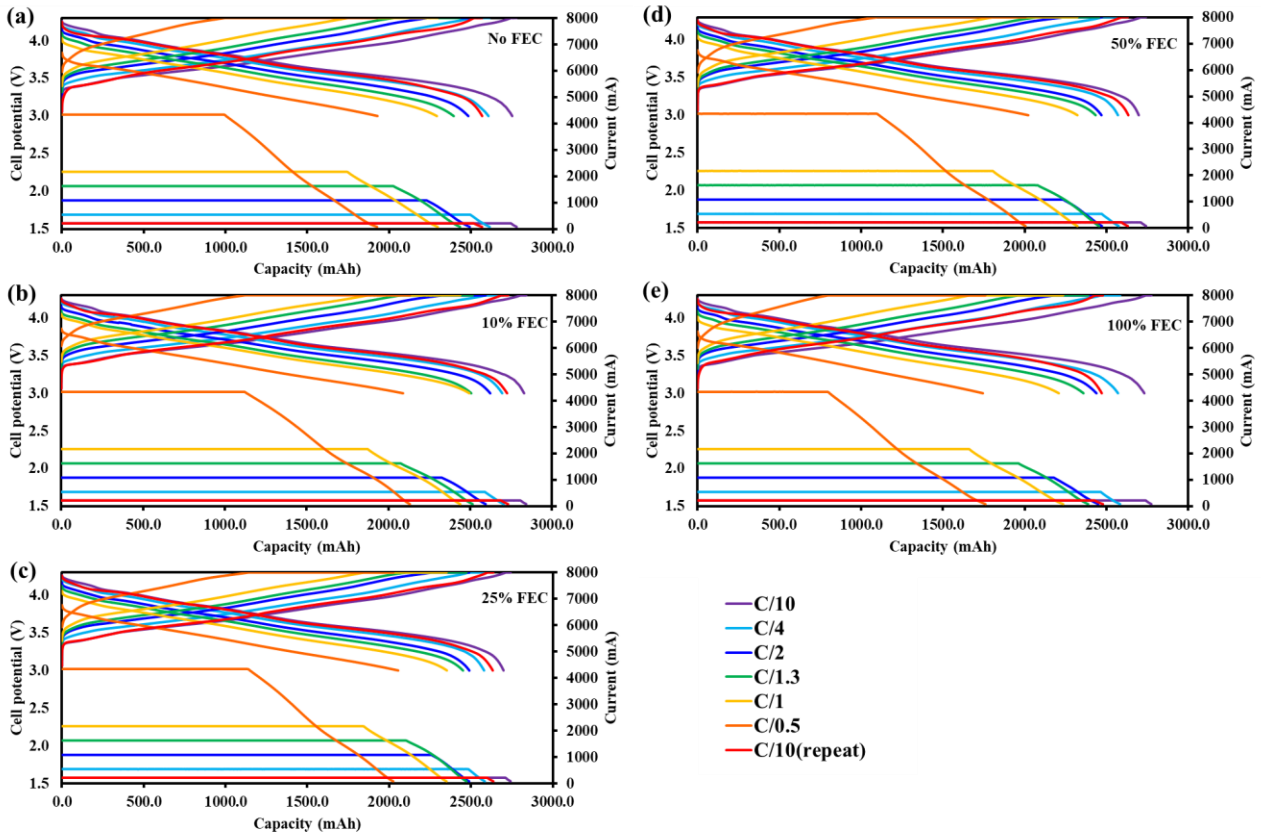

Figure S13. The galvanostatic charge-discharge profile at various C-rate for different FEC conditions

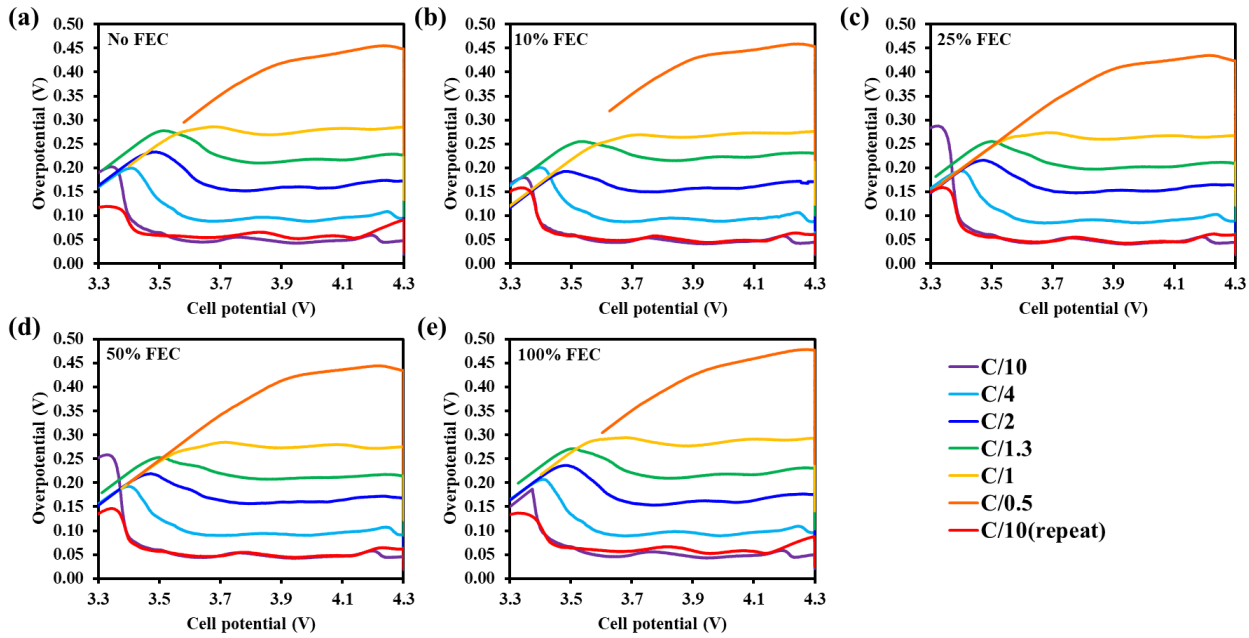

Figure S14. The overpotential plot derived from galvanostatic charge-discharge profile at various C-rate for different FEC conditions.

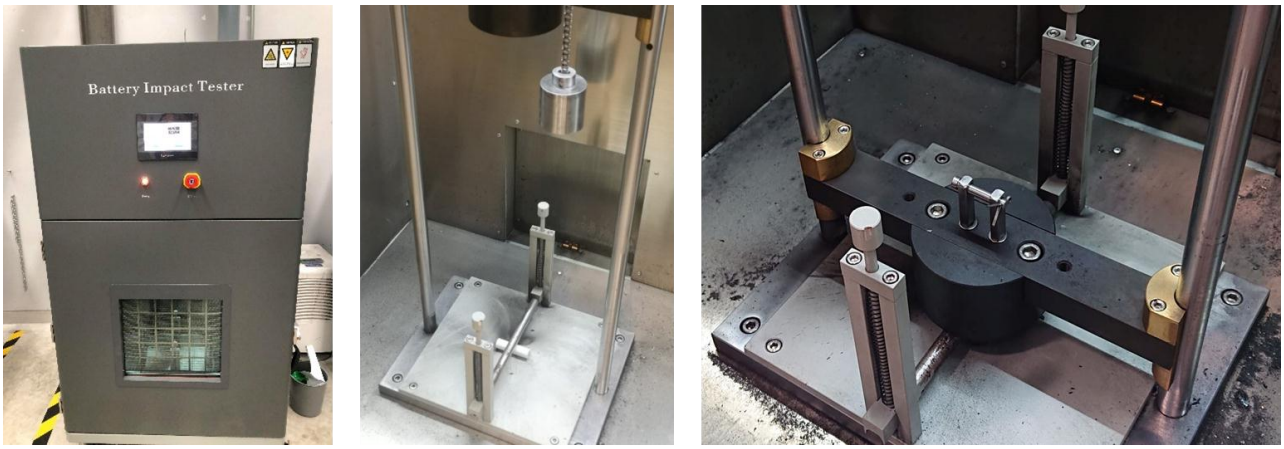

Figure S15. Battery impact tester machine.

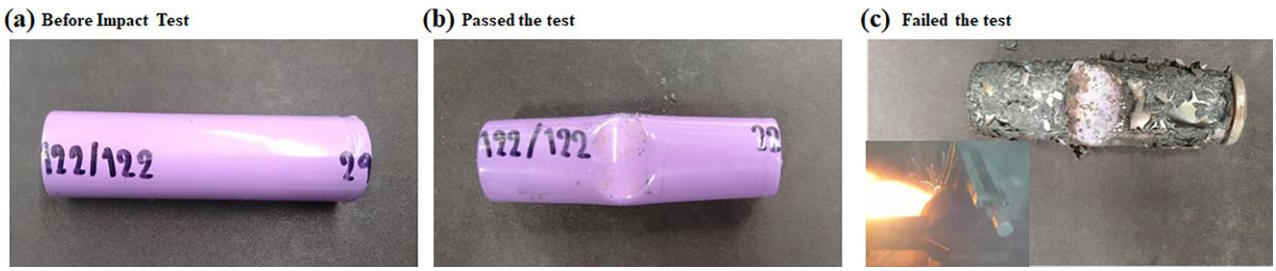

Figure S16. Postmortem photographs of the cylindrical 18650 cells. (a) The example of the cell before the impact test, (b) the example of the passed cell, and (c) the example of the failed cell along with an explosion captured image (inset). All the tested cells were measured after constant-current-constant-voltage (CCCV) charged to 4.3 V at C/10 rate.

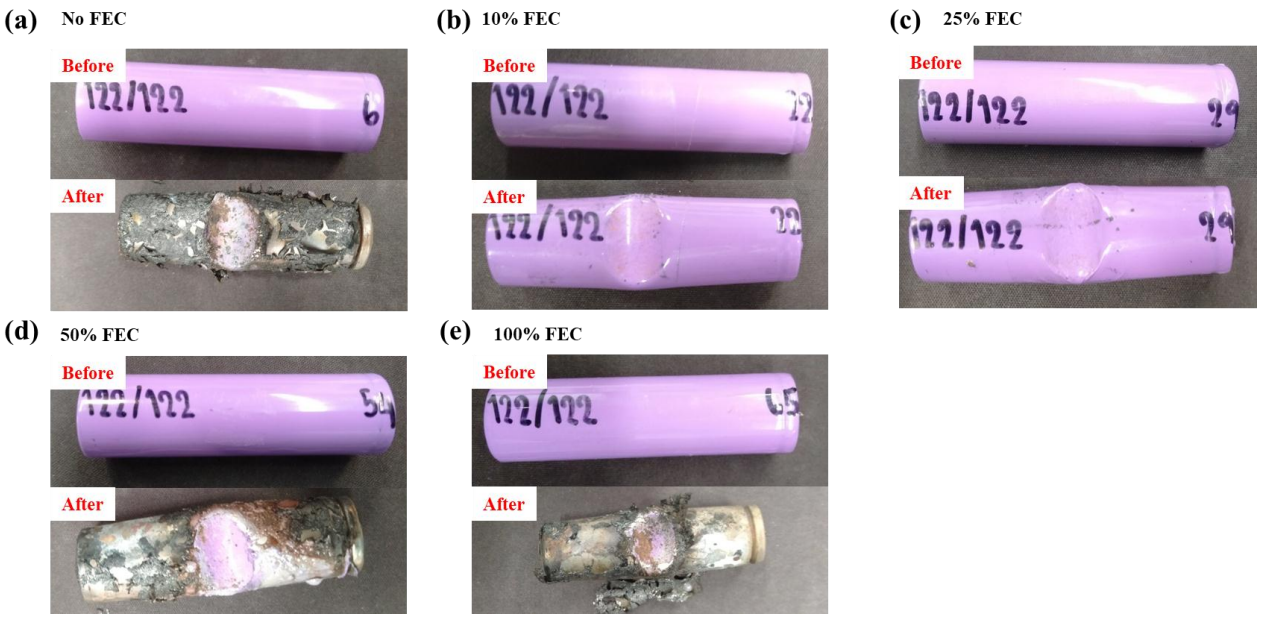

Figure S17. The cylindrical 18650-type lithium-ion battery before and after impact test for (a) no FEC, (b) 10% FEC, (c) 25% FEC, (d) 50% FEC, and (e) 100% FEC.

Table S1. Initial configuration of the simulation cells.

Systems		Li^+	PF_6^-	EC	DEC	EMC	FEC
No FEC	**No. of Molecule**	52	52	274	150	176	0
	%wt.	N/A	N/A	40.1	29.4	30.5	0
10%vol FEC	**No. of Molecule**	52	52	261	144	168	27
	%wt.	N/A	N/A	38.1	28.2	29.0	4.7
25%vol FEC	**No. of Molecule**	52	52	240	132	155	73
	%wt.	N/A	N/A	34.9	25.7	26.6	12.8
50%vol FEC	**No. of Molecule**	52	52	193	106	124	177
	%wt.	N/A	N/A	27.8	20.5	21.1	30.7
100%vol FEC	**No. of Molecule**	52	52	0	0	0	600
	%wt.	N/A	N/A	0	0	0	100.0

Table S2. Calculated coordination number of Li-X pairs from the integration over the *g(r)* to 2.3 Å, total coordination number, contact ion pair (CIP) ratio, and corresponding contact ion pair formation energy (kcal mol^{-1}).

Systems	**Li^+ – Li^+**	**Li^+ – PF_6**	**Li^+ – FEC**	**Li^+ – DEC**	**Li^+ – EMC**	**Li^+ – EC**	**Total C.N.**	**%CIP**	**%SSIP**	**$\Delta_f G_{CIP}$**
No FEC	0.00	0.063	N/A	1.462	1.173	2.701	5.40	6.30	93.70	1.61
10%vol FEC	0.00	0.07	0.108	1.512	1.14	2.534	5.36	7.00	93.00	1.54
25%vol FEC	0.00	0.085	0.283	1.334	1.173	2.536	5.41	8.50	91.50	1.42
50%vol FEC	0.00	0.067	0.868	1.14	1.176	2.17	5.42	6.70	93.30	1.57
100%vol FEC	0.00	0.046	5.588	N/A	N/A	N/A	5.63	4.60	95.40	1.81

Table S3. Specification data sheet for as-fabricated FEC-contained LiBs cylindrical 18650-type. These reported cells are the cell that used for the rate-capability determination.

	No FEC	**10% FEC**	**25% FEC**	**50% FEC**	**100% FEC**
Cell Weight (g)	42.65	43.07	41.87	42.74	42.85
Diameter (mm)	18.20				
Height (mm)	65.00				
Cell Volume (cm^3)	16.50				
Nominal Voltage (V)	3.7	3.7	3.7	3.7	3.7
Capacity (mAh) (After formation)	2794.3	2856.3	2738.0	2739.9	2771.3
Cathode	$LiNi_{0.88}Co_{0.09}Al_{0.03}O_2$ (Gelon Lib., China)				
Cathode current collector	Aluminium foil (Thickness: 7.0 μm, 0.028 g/cm^2)				
Anode	Graphite (Gelon Lib., China)				
Anode current collector	Copper foil (Thickness: 5.6 μm, 0.056 g/cm^2)				
Gravimetric energy density (Wh/kg)	242.4	245.4	242.0	237.2	239.3
Volumetric energy density (Wh/L)	626.6	640.5	614.0	614.4	621.4

Links to safety tests

The cell with highly concentrated FEC.

https://www.dropbox.com/s/0dcofybsbtnnxt9/Video1_Passed.wmv?dl=0

The cell without highly concentrated FEC.

https://www.dropbox.com/s/mqry528lw7t4o02/Video2_Failed.mp4?dl=0

Supplementary References.

1. C. Y. Son, J. G. McDaniel, J. R. Schmidt, Q. Cui and A. Yethiraj, *The Journal of Physical Chemistry B*, 2016, **120**, 3560-3568.
2. M. Takeuchi, Y. Kameda, Y. Umebayashi, S. Ogawa, T. Sonoda, S.-i. Ishiguro, M. Fujita and M. Sano, *Journal of Molecular Liquids*, 2009, **148**, 99-108.
3. K. P. Jensen and W. L. Jorgensen, *Journal of Chemical Theory and Computation*, 2006, **2**, 1499-1509.
4. J. N. Canongia Lopes and A. A. H. Pádua, *The Journal of Physical Chemistry B*, 2004, **108**, 16893-16898.
5. A. D. Becke, *The Journal of Chemical Physics*, 1993, **98**, 5648-5652.
6. M. J. Frisch, G. W. Trucks, H. B. Schlegel, G. E. Scuseria, M. A. Robb, J. R. Cheeseman, G. Scalmani, V. Barone, G. A. Petersson, H. Nakatsuji, X. Li, M. Caricato, A. V. Marenich, J. Bloino, B. G. Janesko, R. Gomperts, B. Mennucci, H. P. Hratchian, J. V. Ortiz, A. F. Izmaylov, J. L. Sonnenberg, Williams, F. Ding, F. Lipparini, F. Egidi, J. Goings, B. Peng, A. Petrone, T. Henderson, D. Ranasinghe, V. G. Zakrzewski, J. Gao, N. Rega, G. Zheng, W. Liang, M. Hada, M. Ehara, K. Toyota, R. Fukuda, J. Hasegawa, M. Ishida, T. Nakajima, Y. Honda, O. Kitao, H. Nakai, T. Vreven, K. Throssell, J. A. Montgomery Jr., J. E. Peralta, F. Ogliaro, M. J. Bearpark, J. J. Heyd, E. N. Brothers, K. N. Kudin, V. N. Staroverov, T. A. Keith, R. Kobayashi, J. Normand, K. Raghavachari, A. P. Rendell, J. C. Burant, S. S. Iyengar, J. Tomasi, M. Cossi, J. M. Millam, M. Klene, C. Adamo, R. Cammi, J. W. Ochterski, R. L. Martin, K. Morokuma, O. Farkas, J. B. Foresman and D. J. Fox, *Journal*, 2016.

7. N. N. Rajput, V. Murugesan, Y. Shin, K. S. Han, K. C. Lau, J. Chen, J. Liu, L. A. Curtiss, K. T. Mueller and K. A. Persson, *Chemistry of Materials*, 2017, **29**, 3375-3379.
8. C. I. Bayly, P. Cieplak, W. Cornell and P. A. Kollman, *The Journal of Physical Chemistry*, 1993, **97**, 10269-10280.
9. L. Martínez, R. Andrade, E. G. Birgin and J. M. Martínez, *Journal of Computational Chemistry*, 2009, **30**, 2157-2164.
10. S. Nosé, *Molecular Physics*, 1984, **52**, 255-268.
11. M. J. Abraham, T. Murtola, R. Schulz, S. Páll, J. C. Smith, B. Hess and E. Lindahl, *SoftwareX*, 2015, **1-2**, 19-25.
12. S. Pronk, S. Páll, R. Schulz, P. Larsson, P. Bjelkmar, R. Apostolov, M. R. Shirts, J. C. Smith, P. M. Kasson, D. van der Spoel, B. Hess and E. Lindahl, *Bioinformatics*, 2013, **29**, 845-854.
13. B. Hess, C. Kutzner, D. van der Spoel and E. Lindahl, *Journal of Chemical Theory and Computation*, 2008, **4**, 435-447.
14. D. Van Der Spoel, E. Lindahl, B. Hess, G. Groenhof, A. E. Mark and H. J. C. Berendsen, *Journal of Computational Chemistry*, 2005, **26**, 1701-1718.
15. E. Lindahl, B. Hess and D. van der Spoel, *Molecular modeling annual*, 2001, **7**, 306-317.
16. H. J. C. Berendsen, D. van der Spoel and R. van Drunen, *Computer Physics Communications*, 1995, **91**, 43-56.
17. A. E. Reed, L. A. Curtiss and F. Weinhold, *Chemical Reviews*, 1988, **88**, 899-926.
18. E. Cancès, B. Mennucci and J. Tomasi, *The Journal of Chemical Physics*, 1997, **107**, 3032-3041.
19. B. Mennucci, R. Cammi and J. Tomasi, *The Journal of Chemical Physics*, 1998, **109**, 2798-2807.
20. S. Miertuš, E. Scrocco and J. Tomasi, *Chemical Physics*, 1981, **55**, 117-129.